Supporting Information for

Evaluating the Identity and Diiron Core Transformations of a (μ-Oxo)diiron(III) Complex Supported by an Electron-Rich Tris(pyridyl-2-methyl)amine Ligand

Loi H. Do[†], Genqiang Xue[‡], Lawrence Que, Jr.[‡] Stephen J. Lippard[†]**

[†]Department of Chemistry, Massachusetts Institute of Technology, Cambridge, MA 02139; lippard@mit.edu
[‡]Department of Chemistry and Center for Metals in Biocatalysis, University of Minnesota, Minneapolis, MN 55455; larryque@umn.edu

Table of Contents **Page(s)**

Table S1. X-ray Data Collection and Refinement Parameters for **2**, **10a**, and **10b**.

	2	**10a**	**10b**
Empirical formula	$[Fe_2N_8O_8C_{54}H_{72}](ClO_4)_3 \cdot (CH_3CN)_4$	$[Fe_2N_8O_9C_{56}H_{75}](ClO_4)_3 \cdot (CH_3CN)_3$	$[Fe_2N_8O_9C_{56}H_{75}](ClO_4)_3 \cdot (CH_3CN)_{2.5}(C_4H_{10}O)_{0.5}$
Formula weight	1535.46	1537.45	1548.94
Temperature (K)	100	100	100
Wavelength (Å)	0.71073	0.71073	0.71073
Crystal system	Monoclinic	Triclinic	Triclinic
Space group	C2/c	$P\bar{1}$	$P\bar{1}$
Unit cell dimensions	a = 28.2258(19) Å b = 11.7652(8) Å c = 22.4938(15) Å β = 106.6850(10)°	a = 13.6256(9) Å b = 14.0402(9) Å c = 20.2928(13) Å α = 81.2320(10)° β = 72.8600(10)° γ = 71.0910(10)°	a = 13.6723(12) Å b = 22.640(2) Å c = 24.640(2) Å α = 99.8960(10)° β = 98.875(2)° γ = 102.9360(10)°
Volume ($Å^3$)	7155.3(8)	3503.6(4)	7135.5(11)
Z	2	2	2
Calculated density (g/mm^3)	1.425	1.458	1.442
Absorption coefficient (mm^{-1})	0.596	0.610	0.600
F(000)	3212	1600	3236
Crystal size (mm^3)	0.32 x 0.17 x 0.13	0.20 x 0.10 x 0.07	0.20 x 0.16 x 0.12
Θ range for data collection	1.51 to 26.73°	1.54 to 26.41°	1.14 to 26.77°
Index ranges	$-35 \le h \le 35$ $-14 \le k \le 14$ $-20 \le l \le 20$	$-16 \le h \le 17$ $-17 \le k \le 17$ $-25 \le l \le 25$	$-17 \le h \le 17$ $-28 \le k \le 28$ $-30 \le l \le 30$
Reflections collected	63728	61129	123942
Independent reflections	7549 [R(int) = 0.0340]	14283 [R(int) = 0.0532]	30171 [R(int) = 0.0564]
Completeness to Θ (%)	99.3	99.4	99.1
Absorption correction	Empirical	Empirical	Empirical
Max. and min. transmission	0.9265 and 0.8321	0.9586 and 0.8878	0.9315 and 0.8895
Data / restraints / parameters	7549/85/473	14283/0/952	30171/4/1808
Goodness-of-fit on F^2	1.077	1.016	1.030
Final R indices [I>2σ(I)]	R1 = 0.0652 wR2 = 0.1759	R1 = 0.0552 wR2 = 0.1259	R1 = 0.0673 wR2 = 0.1747
R indices (all data)	R1 = 0.0722 wR2 = 0.1815	R1 = 0.0810 wR2 = 0.1381	R1 = 0.0967 wR2 = 0.1937
Largest diff. peak and hole (eA^3)	1.828 and -0.693	1.429 and -1.188	2.467 and -1.199

* $R1 = \Sigma\,||F_o|-|F_o||/\Sigma|F_o|$; $wR2 = \{\Sigma[w(F_o^2-F_c^2)^2]/\Sigma[w(F_o^2)^2]\}^{1/2}$; $GOF = \{\Sigma[w(F_o^2-F_c^2)^2]/(n-p)\}^{1/2}$, where n is the number of reflections and p is the total number of parameters refined.

Table S2. Selected Structural Parameters of **10a** and **10b**.

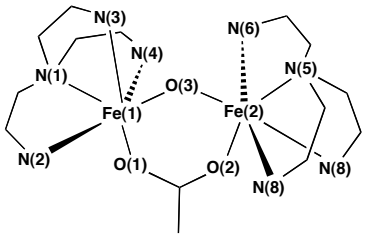

	10a	**10b**[b]
Bond Distances (Å)[a]		
Fe(1)–Fe(4)	3.252(3)	3.250(3), 3.250(3)
Fe(1)–O(1)	2.044(2)	2.042(3), 2.038(3)
Fe(1)–O(3)	1.783(2)	1.794(3), 1.788(3)
Fe(1)–N(1)	2.212(3)	2.216(3), 2.221(3)
Fe(1)–N(2)	2.114(3)	2.137(3), 2.119(3)
Fe(1)–N(3)	2.128(3)	2.135(2), 2.131(3)
Fe(1)–N(4)	2.146(3)	2.138(3), 2.151(3)
Fe(2)–O(2)	1.962(2)	1.984(3), 1.966(3)
Fe(2)–O(3)	1.801(2)	1.808(3), 1.803(3)
Fe(2)–N(5)	2.182(3)	2.191(3), 2.191(3)
Fe(2)–N(6)	2.138(3)	2.121(3), 2.134(3)
Fe(2)–N(7)	2.228(3)	2.228(3), 2.233(3)
Fe(2)–N(8)	2.128(3)	2.131(3), 2.136(3)
Bond Angles (deg)[a]		
Fe(1)–O(3)–Fe(2)	130.15(13)	128.98(15), 129.62(15)
O(3)–Fe(1)–O(1)	98.47(10)	99.63(12), 99.39(12)
O(3)–Fe(2)–O(2)	102.39(10)	102.14(12), 101.70(12)
N(1)–Fe(1)–N(2)	77.70(10)	75.81(12), 76.58(12)
N(1)–Fe(1)–N(3)	79.20(10)	79.01(13), 78.95(13)
N(1)–Fe(1)–N(4)	75.07(10)	76.18(12), 75.59(12)
N(5)–Fe(2)–N(6)	76.09(10)	78.52(12), 77.11(13)
N(5)–Fe(2)–N(7)	77.98(10)	76.93(12), 77.49(12)
N(5)–Fe(2)–N(8)	76.69(10)	75.89(12), 76.98(12)

[a]A generalized numbering scheme, depicted in the above cartoon representation, is used. These atom labels do not necessarily correspond to those assigned in their respective X-ray structures. [b]There are two independent molecules of **10b** in the asymmetric unit; parameters of both cations are given.

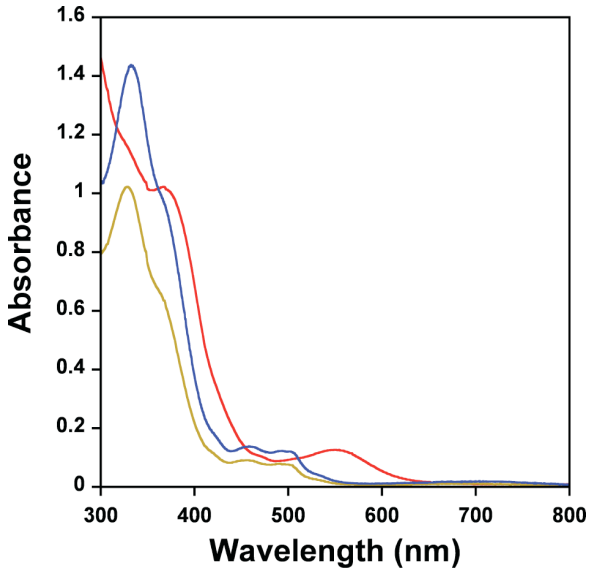

Figure S1. UV-vis spectra of complexes **2** (red), **10a** (yellow), and **10b** (blue) recorded in dichloromethane at RT. Red spectrum: λ_{max} = 370, 550 nm; yellow spectrum: λ_{max} = 332, 454, 492 nm; blue spectrum: λ_{max} = 332, 454, 492 nm. The concentrations of **2**, **10a**, and **10b** are approximately 190, 89, and 58 μM, respectively.

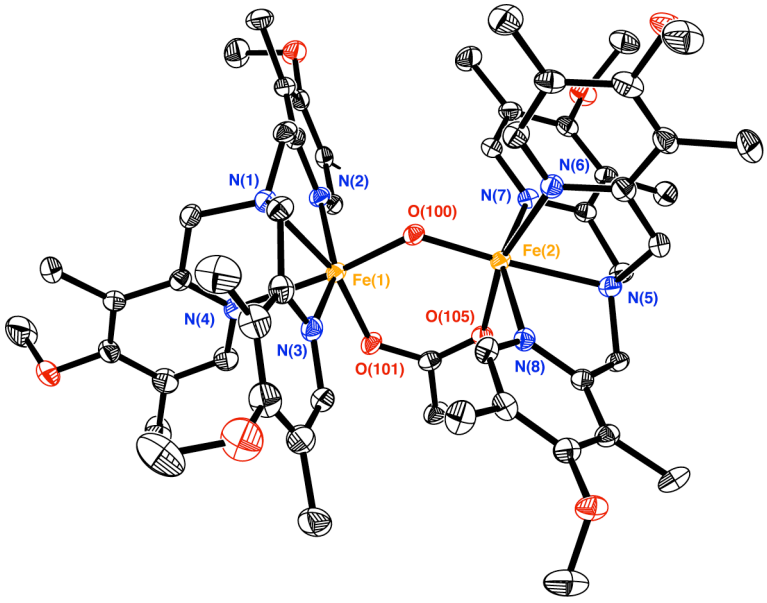

Figure S2. A thermal ellipsoid (50%) diagram of the X-ray structure of $[Fe_2(\mu\text{-}O)(\mu\text{-}CH_3CO_2)(R_3TPA)_2](ClO_4)_3\cdot(CH_3CN)_{2.5}(Et_2O)_{0.5}$ (**10b**). Two independent molecules of **10b** occur in the asymmetric unit. Hydrogen atoms, solvent molecules, and perchlorate anions are omitted for clarity. Color scheme: iron, orange; oxygen, red; nitrogen, blue; carbon, black. See Tables S1 and S2 for data refinement and structural parameters of **10b**, respectively.

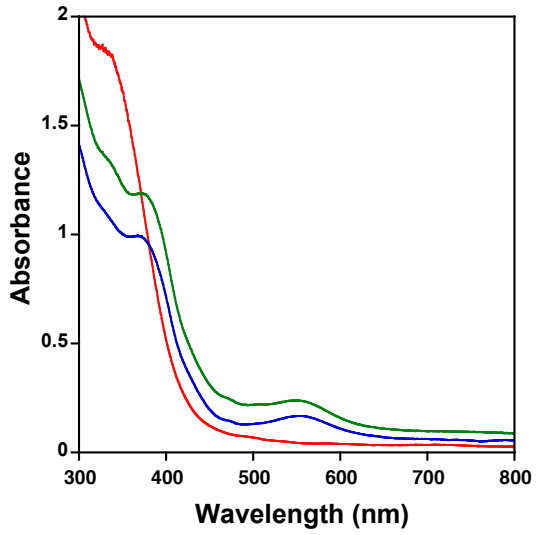

Figure S3. UV-vis spectra of complex **2** recorded in different solvents. The 375 and 550 nm bands are observed in dichloromethane (green) and acetonitrile (blue) but not in a dichloromethane/methanol (1:1) mixture. The diamond core in **2** is maintained only in non-protic solvents.

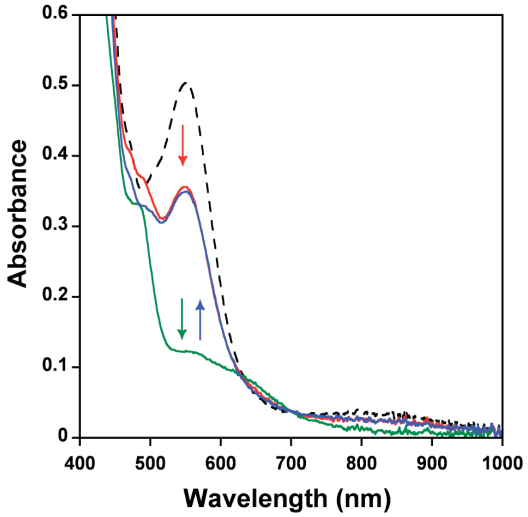

Figure S4. Plot showing the effect of temperature and water on the UV-vis spectrum of a 0.7 mM acetonitrile solution of complex **2**. At RT, **2** displays a prominent band at 550 nm (dashed line). When cooled to -30 °C, this absorption decreases (red) and completely disappears upon addition of ~8,000 equiv of water (green) vs the diiron complex. The band at 550 nm is partially restored upon warming the solution back to RT (blue).

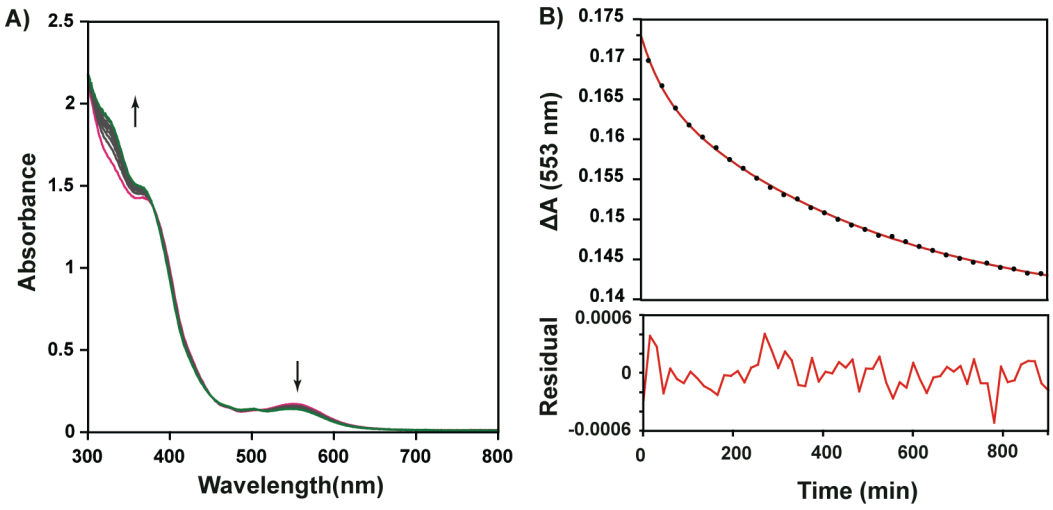

Figure S5. Reaction of **2** in acetonitrile (283 μM) (solvent-grade, not pre-dried) at RT followed by UV-vis absorption spectroscopy. The complete optical profile is shown in panel A. The absorption changes at 553 nm are shown in panel B as black dots. The data were fit to an A→B→C kinetic model (red trace), yielding the parameters: k_1 = 2.04 ± 0.16 x 10^{-2} min^{-1}, k_2 = 1.98 ± 0.06 x 10^{-3} min^{-1}, ε_A = 610.9 ± 0.5 $M^{-1}cm^{-1}$, ε_B = 578.5 ± 1.4 $M^{-1}cm^{-1}$, ε_C = 488.8 ± 1.0 $M^{-1}cm^{-1}$, X^2 = 1.72 x 10^{-6}, and R = 0.99977. See eq. 1 in the Experimental Section for the mathematical expression used.

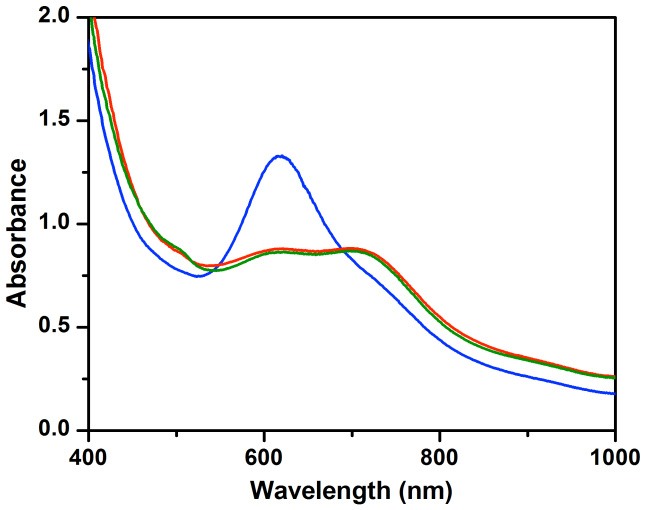

Figure S6. UV-vis spectra of solutions from reactions of 0.5 mM **2** with (1) 0.5 mM H_2O_2 (red solid line), (2) 0.5 mM D_2O_2 + 50 mM D_2O (green solid line), or (3) 0.5 mM H_2O_2 + 50 mM H_2O (blue solid line).

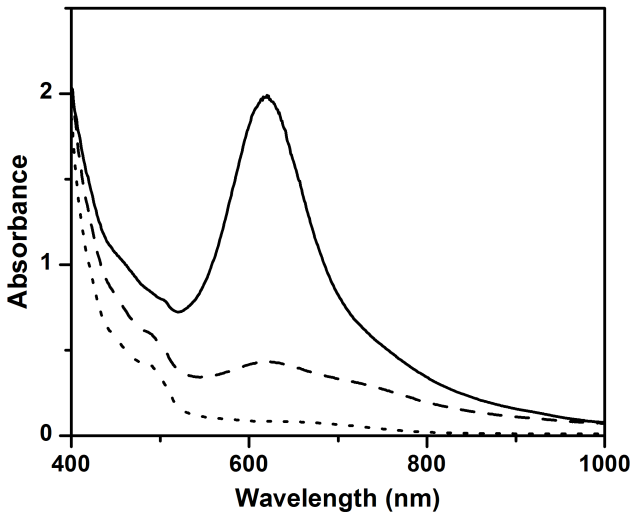

Figure S7. UV-vis spectra of 0.5 mM **2** in acetone (dotted line) and after reaction with 1.0 mM H_2O_2 at -40 ºC for 30 s (dashed line) and 1,000 s (solid). In the dashed line spectrum, an absorption feature at 705 nm can be discerned that shows some formation of intermediate **4**, which reacts with residual H_2O_2 to form $\{Fe^{III}Fe^{IV}(\mu\text{-}O)_2\}^{3+}$ (**7**, λ_{max} = 620 nm). From the solid line we compute a 75% yield of **7** from **2**.

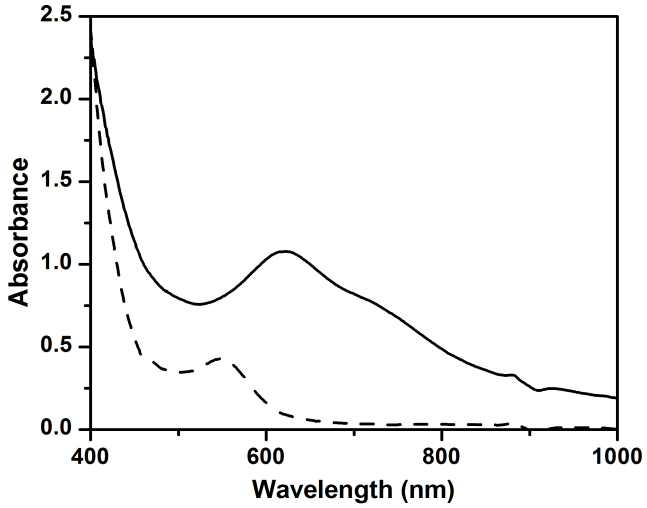

Figure S8. UV-vis spectra of 0.5 mM **2** in 3:1 CH_2Cl_2/CH_3CN (dotted line) and 90 s after reaction with 0.5 mM H_2O_2 (solid line) at -40 ºC. These data show that a significant amount of **7** forms in the reaction of **2** with H_2O_2 in 3:1 CH_2Cl_2/CH_3CN, compared to the observed clean formation of **4** in pure CH_3CN.